

Subcycle engineering of laser filamentation in gas by harmonic seeding

P. Béjot,* G. Karras, F. Billard, J. Doussot, E. Hertz, B. Lavorel, and O. Faucher

*Laboratoire Interdisciplinaire CARNOT de Bourgogne,
UMR 6303 CNRS-Université de Bourgogne, BP 47870, 21078 Dijon, France.*

Manipulating at will the propagation dynamics of high power laser pulses is a long-standing dream whose accomplishment would lead to the control of a plethora of fascinating physical phenomena emerging from laser-matter interaction. The present work represents a significant step towards such an ideal control by manipulating the nonlinear optical properties of the gas medium at the quantum level. This is accomplished by engineering the intense laser pulse experiencing filamentation at the subcycle level with a relatively weak ($\simeq 1\%$) third-harmonic radiation. The control results from quantum interferences between a single and a two-color (mixing the fundamental frequency with its 3rd harmonic) ionization channel. This mechanism, which depends on the relative phase between the two electric fields, is responsible for wide refractive index modifications in relation with significant enhancement or suppression of the ionization rate. As a first application, we demonstrate the production and control of an axially modulated plasma channel that could be used for quasi-phase-matched laser wakefield acceleration.

Since its first observation¹ in gases by Braun *et al.* in 1995, the nonlinear propagation of ultrashort ultra-intense laser pulses, *i.e.* filamentation, has attracted a lot of interest in recent years because of its physical interest^{2–5}, as well as its important applications including terahertz⁶ and supercontinuum⁷ generation, remote sensing⁸, attosecond⁹ and high-harmonics¹⁰ physics, spectroscopy¹¹, machining¹² and lightning protection¹³. The main feature of a filament is its ability to sustain very high intensities (around 50 TW/cm²) over very long distances in contrast with the predictions of linear propagation theory. Controlling at will the natural characteristics of a filament and its by-products (such as, for instance, the plasma channel left in its wake) by means of a single control parameter would make the filamentation process an even more versatile tool for applications. First attempts devoted to control the filament characteristics were realized by using a temporal¹⁴ or a spatial^{15–17} pulse shaper eventually coupled with a closed-loop algorithm. Such methods, based on the engineering of the pulse envelope, successfully controlled either the spectral broadening or the plasma channel position. Another way to control

the filamentation process based on molecular alignment was also reported¹⁸. By manipulating the rotational degree of freedom of molecules with a strong laser pulse, it was shown that the filament length, continuity, and electron density can be manipulated. More recently, it was shown that an energetic Bessel beam co-propagating with a filament can extend by an order of magnitude the length of the latter¹⁹ by continuously refueling it all along its propagation. Based on a previous proposal²⁰, the current work demonstrates that the properties of a filament generated in a gas can be manipulated by controlling the nonlinear optical properties of the medium at the quantum level. The underlying idea relies on a subcycle engineering technique originally used for sub-femtosecond spectroscopy²¹ and for controlling high-harmonic generation²². By seeding the filament with a weak third-harmonic pulse, one can engineer the former at the optical cycle scale. By adjusting the phase of the harmonic field, used as the control parameter, one can alter the ionization yield and the refractive index so as to modulate the attributes of the filament. The technique is first implemented in order to apply a control over the length of the filament and its generated supercontinuum. Then, we demonstrate the production and the control of an axially modulated plasma channel. Such a medium, with tunable periodical optical properties, could be used, *inter alia*, for quasi-phase-matched laser wakefield acceleration or for engineering the temporal trajectories of Airy light bullets. Finally, beyond the control of the nonlinear propagation from microscopic to macroscopic extent by means of a single control parameter, this work casts doubts on the standard model used in the description of the filamentation process.

An atom interacting with a non-resonant intense ultrashort laser pulse can simultaneously absorb a large number of photons, leading to its excitation or eventually to its ionization where a fraction of the bound electronic wavepacket is promoted into the continuum. This electronically excited atom exhibits different optical properties as compared to the initial atom, leading to the modification of the propagation of the laser pulse. In a first experiment, we investigate up to what extent the engineering, at the subcycle scale, of an intense IR-pulse with a weak third harmonic beam can modify the optical properties of a gas. The experimental setup used to measure the nonlinear properties of argon is depicted in Fig.1a. The optical source is a 1 kHz amplified femtosecond laser delivering horizontally polarized, 3 mJ, 100 fs pulses at $\lambda_0=796$ nm. The refractive index change induced by the IR pump-beam in a static cell filled with argon at 0.5 bar is measured by the

* pierre.bejot@u-bourgogne.fr

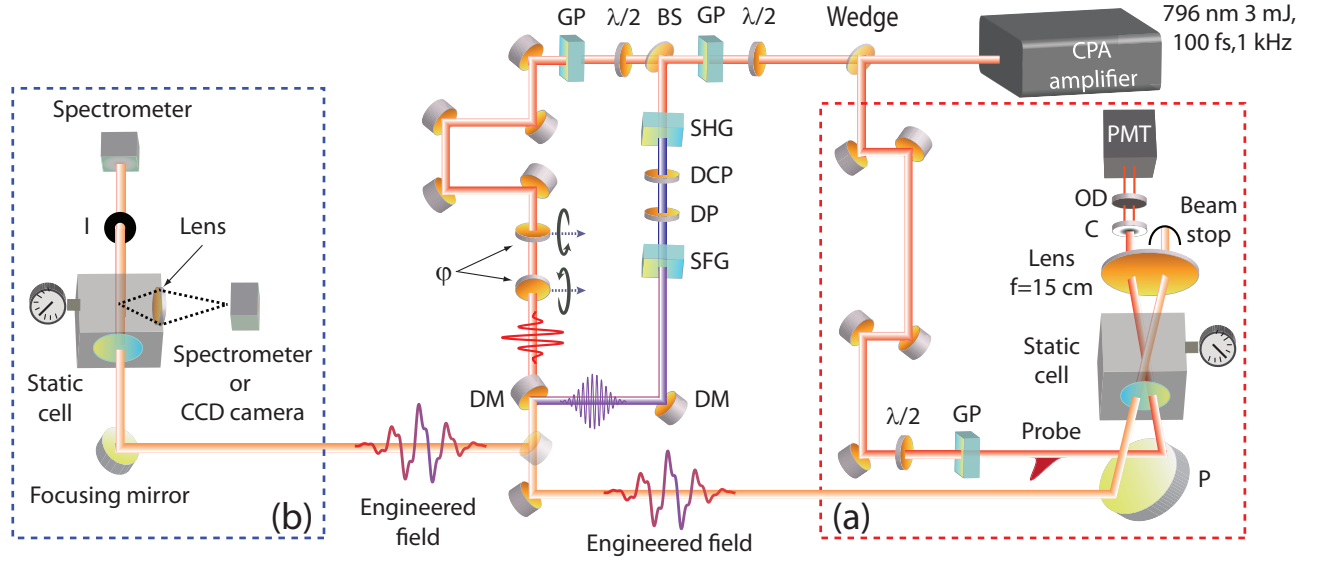


Figure 1. **Experimental realization of the electric field engineering.** Setup for laser-induced cross-defocusing measurements (a) and for the coherent manipulation of a filament produced in argon (b). BS: Beam Splitter, GP: Glan Polarizer, OD: Neutral Optical Density, PMT: Photo Multiplier Tube, DM: Dichroic mirror, C: Coronagraph, DCP: Delay Compensation Plate, DP: Dual Plate ($\lambda/2$ @796 nm, λ @398 nm), P: Parabolic mirror, I: Iris, SHG: Second-Harmonic Generation, SFG: Sum-Frequency Generation.

pump-probe cross-defocusing technique^{23,24}. All the beams are focused with a $f=15$ cm off-axis parabolic aluminium mirror to avoid both longitudinal and lateral chromatism. A third beam with central wavelength $\lambda_{UV} = \lambda_0/3$ is generated by sum-frequency generation itself generated by second-harmonic generation. It is spatially superimposed with the IR pulse by means of a dichroic mirror. The temporal synchronization of the IR and UV pulses is accomplished with the help of a delay line. The polarization of all beams is set vertical with half-wave plates. The cross-defocusing technique relies on the fact that the pump modifies the propagation of the probe pulse by inducing a spatial change on the local refractive index. After the cell, a coronagraph is inserted in the probe beam path. When the pump beam is switched off, the coronagraph obstructs the probe. On the contrary, if the pump beam induces a local refractive index modification, the probe beam size increases in the far field so that a small amount can propagate around the coronagraph. The remaining part of the probe beam is redirected to a photomultiplier tube. One can show that the defocusing signal is proportional to Δn^2 , *i.e.*, the square of the peak to valley change of refractive index experienced by the probe beam²³. When the pump pulse precedes the arrival of the probe, the cross-defocusing signal is proportional to the square of refractive index change resulting from the ionization mechanism and accordingly proportional to the square of the amount of free electrons generated by the pump²⁴. It then allows a direct experimental

measurement of the latter. The subcycle engineering of the pump pulse is realized by controlling the relative phase between the pump and the UV pulses. Such a phase control is accomplished by inserting into the pump optical path two fused silica plates that rotate symmetrically with respect to a plane perpendicular to the propagation direction. Rotating the two plates then slightly modulates the optical path length and accordingly the relative phase φ between the two pulses, leaving the beam pointing direction unchanged.

Results

Figures 2a-d show the modification of the ionization yields induced by the presence of the UV. The red (resp. blue) curves depict the ionization as a function of the UV beam energy when the two electric fields are in phase (resp. out-of-phase). The insets in Figs. 2a,c display the ionization yields as a function of φ . While at low energy (Figs. 2a,b), the ionization yield increases for any phase, at higher energies (Figs. 2c,d), just adding less than 2 % of UV leads to a decrease (up to 50 %) when the two electric fields are out-of-phase. Moreover, the maximal gain on the ionization yield is higher at lower IR intensity. This behavior is in qualitative agreement with the theoretical predictions shown in Figs. 2e,f that depict the ionization yield as a function of both pump and UV intensities for in-phase (Fig. 2e) and out-of-phase electric fields (Fig. 2f). The theoretical results have been obtained by solving the three dimensional time-dependent Schrödinger equation capturing the quantum dynamics of argon in the single active electron approximation. As recently theoretically studied²⁰, the modulation

of the ionization yield observed in Fig.2 results from quantum interferences between two ionization channels: one involving only IR photons and the other mixing IR and a single-UV photons. The confirmation of this effect opens new possibilities for controlling the propagation dynamics of ultra-intense laser pulses and, consequently, all the underlying applications deriving from it.

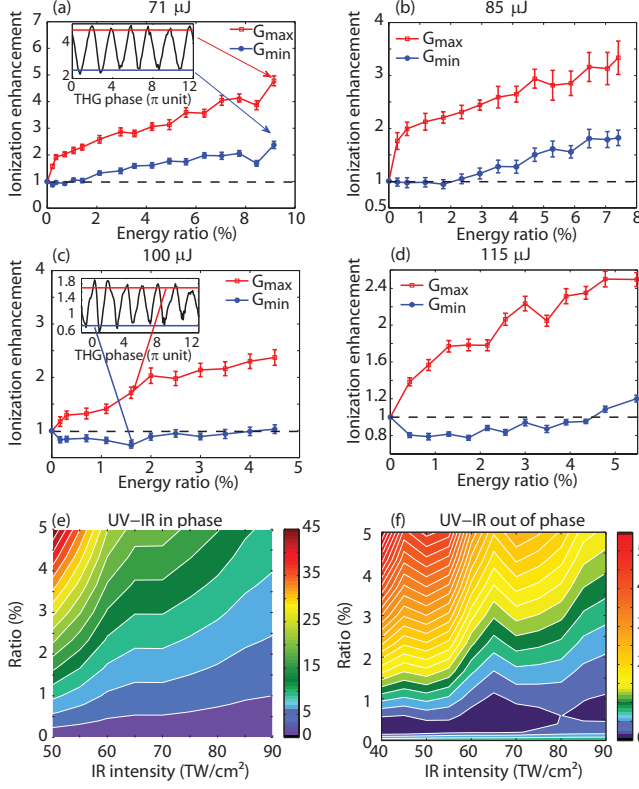


Figure 2. Modification of the nonlinear optical properties of argon by harmonic seeding. **a-d**, Ionization yields as a function of the UV energy (expressed in % of the energy of the IR pulse) for different IR energies E_{IR} (**a**) 71 μJ, (**b**) 85 μJ, (**c**) 100 μJ, and (**d**) 115 μJ. The peak intensities I_{IR} (expressed in TW/cm²) can be approximated by $I_{\text{IR}} \simeq 0.5E_{\text{IR}}$, where E_{IR} is expressed in μJ. The red (blue) curves correspond to the relative phase maximizing (minimizing) the ionization yield. The insets show the experimental ionization yield modification as a function of the relative phase between the two electric fields. For each point, the relative phase between pump and UV beams has been varied over 12 π . The error bars correspond to one standard deviation of the ionization yield modification measured over the full relative phase range. **e,f**, Calculated ionization yields as a function both IR and UV intensities for constructive (**e**) and destructive (**f**) interferences. The calculations have been performed with a 20 cycles laser pulse in order to reduce the computation time.

In order to explore such a possibility, we performed a second experiment where a filament co-propagates with a weak UV beam. The experimental setup is shown in Fig. 1b. An 1 mJ 100 fs IR beam is focused together with a 30 μJ UV pulse in the static cell filled

with argon. Then, the spectrum of the filament that has experienced a strong broadening due to nonlinear propagation is recorded. In order to avoid the saturation of the spectrometer, the spectral region lying between 750 and 850 nm is filtered out with a bandpass filter. At the same time, the fluorescence of the plasma channel is imaged by the side of the cell with the help of a $f=5$ cm lens placed at a distance $2f$ from the plasma channel and a charge-coupled device camera. In order to confirm that the signal collected by the camera was only due to fluorescence and not to laser scattering, a spectrometer was first put in place of the camera. The camera and the two spectrometers are synchronously triggered with the stepper motor used to rotate the two fused silica plates, allowing to record the laser spectrum, the plasma channel, and the gas fluorescence spectrum as a function of the relative phase between the two electric fields. One has to emphasize that, because of the optical refractive index dispersion, the UV and IR electric fields travel with different phase velocities. As a consequence, the relative phase between the two pulses does not remain constant all along the propagation. More particularly, one can define the rephasing length l_{reph} as

$$l_{\text{reph}} = \lambda_{\text{UV}} \left(\frac{1}{n(\lambda_{\text{UV}}) - n(\lambda_0)} \right) \quad (1)$$

where $n(\lambda_0)$ (resp. $n(\lambda_{\text{UV}})$) is the refractive index of the gas at the IR (resp. UV) laser central wavelength. After a propagation over a distance l_{reph} , φ increases by 2π . For a pressure of 1 bar, $l_{\text{reph}} \simeq 1$ cm. In order to explore the dephasing effect, experiments have been performed with both tightly ($f=15$ cm) and loosely ($f=50$ cm) focused beams. In the former (resp. latter) case, the filament is about 2 mm (resp. 6 cm) long, and is consequently shorter (resp. longer) than l_{reph} .

Figure 3a (resp. figure 3b) displays the longitudinal profile of the plasma channel (resp. the laser spectrum) as a function of the relative phase between the two electric fields obtained in the tight focusing geometry. In this regime, the relative phase between the two electric fields remains almost constant over the filament length (about 2 mm). Depending on the φ -value, the filament and the plasma left in its wake experience a strong reshaping. In particular, the supercontinuum generated during the filamentation process gets broader when the harmonic field is in phase with the IR field. As shown in Fig. 3c, the length and density of the plasma channel strongly depend on φ . When the two electric fields are in phase (resp. out of phase), the plasma channel is about 40% shorter (resp. longer) as compared to the IR field alone. Modulation of the plasma length is attended by an 80% increase (or a 10% decrease) of the maximal plasma density depending on the applied relative phase. Moreover, the filament position depends also on φ , as depicted in Fig. 3d. The two extremal cases that correspond to constructive ($\varphi=0$) and destructive ($\varphi=\pi$) quantum interferences are shown in more detail in Figs. 3e-i. When $\varphi=0$ (resp. $\varphi=\pi$), the filament is more intense and shorter (resp. less intense and longer with a double humps structure) than when the UV is switched off.

Figure 4a shows the plasma channel profile along the propagation direction as a function of φ obtained

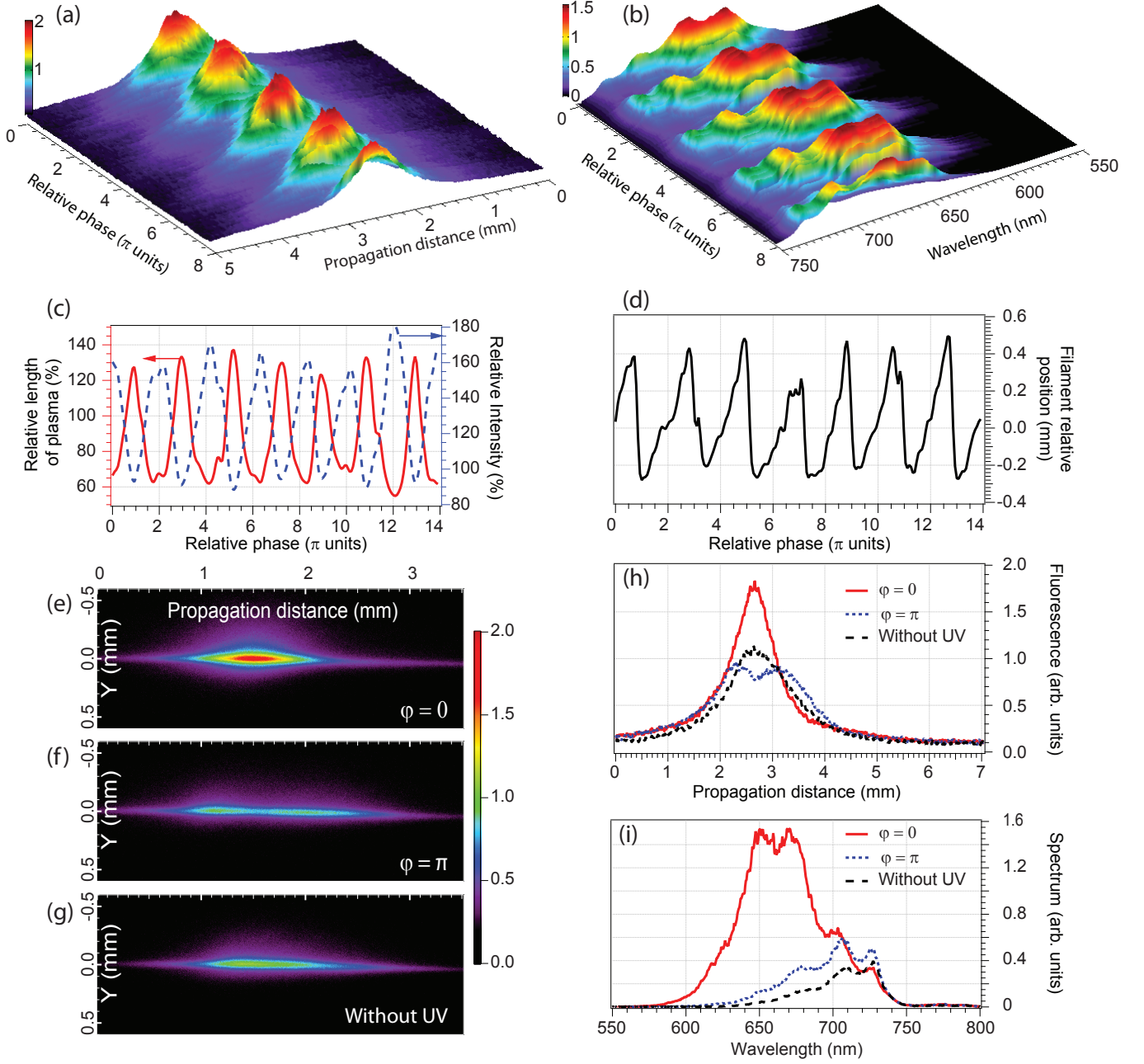


Figure 3. **Control of a filament by subcycle engineering in the tightly focused regime.** **a-d**, Modification of the filament properties as a function φ . **a**, Longitudinal profile of the plasma column. **b**, Supercontinuum generation. **c**, Plasma column length (solid red) and fluorescence (dashed blue). **d**, Filament position. **e-g**, Image of the filament for constructive (**e**) and destructive (**f**) quantum interferences between the different ionization channels compared to the case where the filament propagates without the control UV pulse (**g**). The corresponding longitudinal profiles and spectra are shown in (**h**) and (**i**). The pressure is 1.5 bar.

in the loose focusing geometry at ambient pressure and temperature conditions. In this case, φ does not remain constant over the whole filament length (about 6 cm). The two electric fields experience several periodic rephasing/dephasing cycles, with the period determined by the difference between their respective phase velocities. As a consequence, the plasma channel is axially

modulated with a modulation period of $l_{\text{reph}} \simeq 1$ cm. By tuning the initial relative phase between the two electric fields, the plasma channel extrema position continuously shifts along the propagation distance. As depicted in Fig. 4b, the period can be controlled by adjusting the pressure, *i.e.*, by changing the phase velocity mismatch between the two electric fields. As shown in Fig. 4c, the

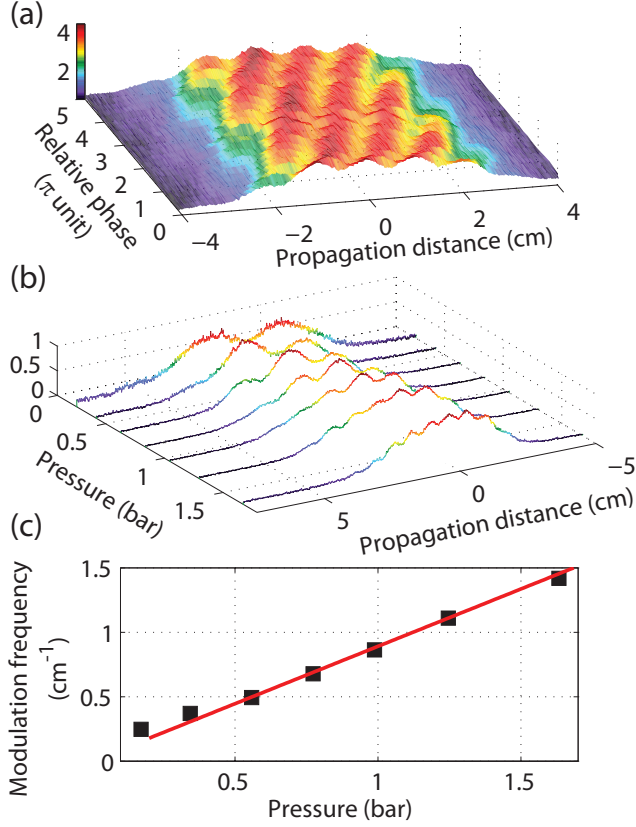


Figure 4. **Production and control of an axially modulated plasma channel in the loose focusing regime.** **a-b**, Longitudinal profile of the plasma channel as a function of φ for a pressure of 1 bar **(a)** and as a function of the pressure **(b)**. **(c)**, Experimental (black squares) and theoretical (red solid line) modulation frequency of the plasma channel as a function of the pressure.

modulation frequency increases linearly with pressure. The production and the control of an axially modulated plasma channel is promising for applications. For instance, the possibility to create a medium with tunable periodical optical properties could be used, *inter alia*, for quasi-phase-matched laser wakefield acceleration²⁵ without the use of an external waveguide, for engineering the temporal trajectories of Airy light bullets²⁶, or for micromachining various periodic optical elements such as waveguides or gratings in the bulk of dielectric media²⁷.

Discussion

Simulating laser pulse propagation over macroscopic distances in a medium undergoing ionization is complicated by the need to include quantum-mechanical laser-atom dynamics. While ionization yield calculations in atoms are routinely performed on the framework of the time-dependent Schrödinger equation, its consideration in the context of two-dimensional laser propagation requires prohibitive numerical resources. For this reason, standard filamentation codes approximate the ionization yield using a simplified analytic formula²⁸ originally developed for purely monochromatic laser fields. Additionally, propagation models accounting for both fundamental and third-harmonic radiations so far

neglect the interferences occurring between the different ionization channels^{29–33}. Besides the experimental demonstration showing that the quantum control of the filamentation process can be performed by seeding the filament with a weak harmonic beam, this work then questions the current theoretical framework on which filamentation simulation is based. Specifically, the present results clearly go beyond the validity range of the theoretical models used for describing the filamentation process and highlight that neglecting the interference effect is not valid even when the UV intensity is only a few percent of the fundamental one. Moreover, while the present experimental results have been obtained by externally seeding the filament with a third-harmonic beam, it is known that the latter is generated at the percent level during the propagation of a filament^{29,30}. A rational question arising from the present work is up to what extent the self-induced third-harmonic can impact the propagation dynamics of a filament by the exhibited UV-IR interference effect. This question will find an answer only after an accurate model of two-color ionization will be available. We hope this work will stimulate theoretical developments toward this direction.

In summary, we have experimentally and theoretically demonstrated that the nonlinear optical properties of a gas experienced by a strong ultrashort laser pulse can be manipulated by a subcycle engineering of the latter. The control has been realized by adding a realistically weak third-harmonic beam that propagates together with the intense laser pulse. Because of quantum interferences occurring during the ionization process, the ionization yield can be either suppressed or enhanced depending on the relative phase between the two electric fields. We have applied this concept to the control of the nonlinear propagation dynamics of a strong laser beam experiencing filamentation. More particularly, we have succeeded in manipulating the supercontinuum generation and the plasma column properties, such as its length and amplitude by adjusting the relative phase between the two electric fields. Moreover, taking advantage of the phase velocity mismatch between the two electric fields, we have created and controlled a sinus-like plasma channel that could be used for quasi-phase-matched laser wakefield acceleration. Demonstrated in argon gas, the control of filamentation by field engineering is based on a non-resonant quantum process. As such, it is a versatile technique that could be applicable to any gas and even to be extended to bulk materials.

Methods

Phase control by two fused silica plates. Considering an incidence angle θ , the optical delay τ induced by inserting two plates of thickness e and refractive index n in the optical path of a pulse is given by:

$$\tau = \frac{2e}{c} \frac{n - \cos(\theta - \arcsin(\frac{\sin \theta}{n}))}{\sqrt{1 - \sin^2 \theta / n^2}}. \quad (2)$$

A rotation $d\theta$ of the two plates around θ_0 induces a relative delay $d\tau$ given by :

$$d\tau \simeq \frac{\partial \tau}{\partial \theta} \bigg|_{\theta_0} \cdot d\theta + \frac{1}{2} \frac{\partial^2 \tau}{\partial \theta^2} \bigg|_{\theta_0} \cdot d\theta^2, \quad (3)$$

with

$$\frac{\partial \tau}{\partial \theta} = \frac{2e}{c} \sin \theta \left(1 - \frac{\cos \theta}{n \sqrt{1 - \sin^2 \theta / n^2}} \right). \quad (4)$$

Around $\theta = 0$, the delay is a slowly varying nonlinear function of the rotation angle, whereas at large angle it is almost linear with θ but with less resolution. Assuming that the angular resolution given by the minimal step of the motor is about $4.5 \cdot 10^{-5}$ radian, tilting the angle between 10 and 20° could allow a temporal

sampling of 30 points per third-harmonic optical cycle, *i.e.* an 30 as resolution in the relative delay between the IR and UV pulses. In order to calibrate the phase change induced by rotating the plates, we inserted them into an HeNe laser-based Michelson interferometer. The interference pattern was then analyzed as a function of the rotation of the plates which provided a direct calibration of the phase control setup.

Numerical methods. The population promoted into the continuum after the interaction was evaluated by solving the time-dependent Schrödinger equation³⁴. Calculations were performed in argon under the single-active electron approximation. Within the dipole and single active electron approximations, the three dimensional time-dependent Schrödinger equation describing the evolution of the electron wavefunction $|\psi\rangle$ in the presence of an electric field $\mathbf{E}(t)$ reads:

$$i\frac{d|\psi\rangle}{dt} = (H_0 + H_{\text{int}})|\psi\rangle, \quad (5)$$

where $H_0 = \nabla^2/2 + V_{\text{eff}}$ is the atom Hamiltonian, $H_{\text{int}} = \mathbf{A}(t) \cdot \boldsymbol{\pi}$, where $\mathbf{A}(t)$ is the vector potential such that $\mathbf{E}(t) = -\partial\mathbf{A}/\partial t$ and $\boldsymbol{\pi} = -i\nabla$ is the interaction term expressed in the velocity gauge. The effective potential V_{eff} of argon used in the calculation accurately fits the argon eigen-energies and -wavefunctions³⁵. The time-dependent wavefunction $|\psi\rangle$ is expanded on a finite basis of B-splines allowing memory efficient fast numerical calculations with

a very large basis set³⁶:

$$\psi(\mathbf{r}, t) = \sum_{l=0}^{l_{\text{max}}} \sum_{i=1}^{n_{\text{max}}} c_i^l(t) \frac{B_i^k(r)}{r} Y_l^0(\theta, \phi), \quad (6)$$

where B_i^k and Y_l^m are B-spline functions and spherical harmonics, respectively. The basis parameters (l_{max} , n_{max} , k and the spatial box size) and the propagation parameters are chosen to ensure convergence. The atom is initially in the ground state (3p) and the electric field E is linearly polarized along the z axis and is expressed as $E(t) = E_0 \cos^2(t/\sigma_t) \sin(\omega_0 t)$ for $|t| < \pi N/\omega_0$, where ω_0 is the central frequency of the laser, $\sigma_t = 2N/\omega_0$, and N the total number of optical cycles within the pulse. The simulations are performed for a laser wavelength of 800 nm and a pulse duration corresponding to $N=20$ cycles. The third-harmonic electric field is expressed as $E_{\text{TH}}(t) = \sqrt{R}E_0 \cos^6[t/\sigma_t] \sin[3\omega_0 t + \varphi]$, where φ is the relative phase between fundamental and third-harmonic electric fields and R is the relative intensity of the third harmonic with respect to the fundamental. Ionization yield induced by either a single IR beam or the combination of UV and IR beams were evaluated as a function of both IR and UV peak intensities for $\varphi = 0$ and $\varphi = \pi$. Note that with this definition of the electric field, based on sinus functions, constructive (resp. destructive) interference is achieved when $\varphi = \pi$ (resp. $\varphi = 0$) unlike the definition used in the figures shown all along the manuscript.

-
- [1] Braun, A. *et al.* Self-channeling of high-peak-power femtosecond laser pulses in air. *Opt. Lett.* **20**, 73-75 (1995).
 - [2] Chin, S.L. *et al.* The propagation of powerful femtosecond laser pulses in optical media: physics, applications, and new challenges. *Can. J. Phys.* **83**, 863-905 (2005).
 - [3] Bergé, L. *et al.* Ultrashort filaments of light in weakly ionized, optically transparent media. *Rep. Prog. Phys.* **70**, 1633 (2007).
 - [4] Couairon, A. & Mysyrowicz, A. Femtosecond filamentation in transparent media. *Phys. Rep.* **441**, 47-189 (2007).
 - [5] Kasparian, J. & Wolf, J.-P. Physics and applications of atmospheric nonlinear optics and filamentation. *Opt. Express* **16**, 466-493 (2008).
 - [6] D'Amico, C. *et al.* Conical Forward THz Emission from Femtosecond-Laser-Beam Filamentation in Air. *Phys. Rev. Lett.* **98**, 235002 (2007).
 - [7] Akozbek, N., Scalora, M., Bowden, C.M. & Chin, S.L. White-light continuum generation and filamentation during the propagation of ultra-short laser pulses in air. *Optics Comm.* **191**, 353-362 (2001).
 - [8] Kasparian, J. *et al.* White-Light Filaments for Atmospheric Analysis. *Science* **301**, 61-64 (2003).
 - [9] Couairon, A. *et al.* From single-cycle self-compressed filaments to isolated attosecond pulses in noble gases. *Phys. Rev. A* **77**, 053814 (2008).
 - [10] Steingrube, D.S. *et al.* High-order harmonic generation directly from a filament. *New J. of Phys.* **13**, 043022 (2011).
 - [11] Stelmaszczyk, K. *et al.* Long-distance remote laser-induced breakdown spectroscopy using filamentation in air. *Appl. Phys. Lett.* **88**, 3977-3979 (2004).
 - [12] Kiselev, D., Woeste, L. & Wolf, J.-P. Filament-induced laser machining. *Appl. Phys. B* **100**, 515-520 (2010).
 - [13] Kasparian, J. *et al.* Electric events synchronized with laser filaments in thunderclouds. *Opt. Express* **16**, 5757-5763 (2008).
 - [14] Ackermann, R. *et al.* Optimal control of filamentation in air. *Appl. Phys. Lett.* **89** (2006)
 - [15] Heck, G., Sloss, J. & Levis, R.J. Adaptive control of the spatial position of white light filaments in an aqueous solution. *Opt. Comm.* **259**, 216222 (2006)
 - [16] Pfeifer, T. *et al.* Circular phase mask for control and stabilization of single optical filaments. *Opt. Lett.* **31**, 2326-2328 (2006)
 - [17] Walter, D. *et al.* Spielmann Spatial optimization of filaments. *Appl. Phys. B* **88**, 175-178 (2007)
 - [18] Varma, S., Chen, Y.-H. & Milchberg, H.M. Trapping and Destruction of Long-Range High-Intensity Optical Filaments by Molecular Quantum Wakes in Air *Phys. Rev. Lett.* **101**, 205001 (2008)
 - [19] Scheller, M. *et al.* Externally refuelled optical filaments. *Nat. Phot.* **8**, 297-301 (2014)
 - [20] Béjot, P. *et al.* Harmonic Generation and Nonlinear Propagation: When Secondary Radiations Have Primary Consequences. *Phys. Rev. Lett.* **112**, 203902 (2014)
 - [21] Wirth, A. *et al.* Synthesized Light Transients. *Science* **334**, 195 (2011)
 - [22] Haessler, S. *et al.* Optimization of Quantum Trajectories Driven by Strong-Field Waveforms. *Phys. Rev. X* **4**, 021028 (2014)
 - [23] V. Renard, V., Faucher, O. & Lavorel B. Measurement of laser-induced alignment of molecules by cross defocusing. *Opt. Lett.* **30**, 13429 (2005)
 - [24] Lorient, V. *et al.* Strong-field molecular ionization: determination of ionization probabilities calibrated with field-free alignment. *Opt. Lett.* **31**, 2897-2899 (2006)
 - [25] Yoon, S.J., Palastro, J.P. & Milchberg, H.M. Quasi-Phase-Matched Laser Wakefield Acceleration. *Phys. Rev. Lett.* **112**, 134803 (2014)
 - [26] Wang, S., Fan, D., Bai, X. & Zeng, X. Propagation dynamics of Airy pulses in optical fibers with periodic dispersion modulation. *Phys. Rev. A* **89**, 023802 (2014)
 - [27] Kondo, Y. *et al.* Fabrication of long-period fiber gratings by focused irradiation of infrared femtosecond laser pulses. *Opt. Lett.* **24** 646-648 (1999)
 - [28] Perelomov, A.M., Popov, V.S. & Terentev, M.V. Ionization of atoms in an alternating electric field. *Sov. Phys. JETP* **23**, 924-934 (1966)
 - [29] Bergé, L. *et al.* Supercontinuum emission and enhanced self-guiding of infrared femtosecond filaments sustained by third-harmonic generation in air. *Phys. Rev. E* **71**, 016602 (2005)
 - [30] Aközbe, N. *et al.* Third-Harmonic Generation and Self-Channeling in Air Using High-Power Femtosecond Laser

- Pulses. *Phys. Rev. Lett.* **89**, 143901 (2002)
- [31] Liu, Y. *et al.* Efficient generation of third harmonic radiation in air filaments: A revisit. *Opt. Comm.* **284**, 4706-4713 (2011)
 - [32] Gaarde, M.B. & Couairon, A. Intensity Spikes in Laser Filamentation: Diagnostics and Application. *Phys. Rev. Lett.* **103**, 043901 (2009)
 - [33] Kolesik, M., Wright, E.M. & Moloney, J.V. Supercontinuum and third-harmonic generation accompanying optical filamentation as first-order scattering processes. *Opt. Lett.* **32**, 2816-2818 (2007)
 - [34] Béjot, P. *et al.* High-Field Quantum Calculation Reveals Time-Dependent Negative Kerr Contribution. *Phys. Rev. Lett.* **110**, 043902 (2013)
 - [35] Muller, H.G. Numerical simulation of high-order above-threshold-ionization enhancement in argon. *Phys. Rev. A* **60**, 1341-1350 (1999)

- [36] Bachau, H. *et al.* Applications of B-splines in atomic and molecular physics. *Rep. Prog. Phys.* **64**, 1815-1942 (2001)

Acknowledgements

This work was supported by the Conseil Régional de Bourgogne (PARI program), the CNRS, the French National Research Agency (ANR) through the CoConicS program (contract ANR-13-BS08-0013) and the Labex ACTION program (contract ANR-11-LABX-0001-01). P.B. thanks the CRI-CCUB for CPU loan on its multiprocessor server. The authors gratefully acknowledge V. Tissot and J.-M. Muller for the cell conception and Prof. D. Charalambidis for discussions.

Authors contributions

P.B. suggested the idea of the filamentation control by harmonic seeding. P.B. and J.D. performed the simulations. P.B., G.K. and F.B. performed the experiments. All authors contributed equally to the writing of this work.